Will It Be Beneficial To Simulate the Antifreeze Proteins at Ice Freezing Condition or at Lower Temperature?

ARTICLE *in* THE JOURNAL OF PHYSICAL CHEMISTRY B · AUGUST 2015

Impact Factor: 3.3 · DOI: 10.1021/acs.jpcb.5b04919 · Source: PubMed

2 AUTHORS, INCLUDING:

Anirban Bhunia
Bose Institute
67 PUBLICATIONS **915** CITATIONS

SEE PROFILE

THE JOURNAL OF PHYSICAL CHEMISTRY B

Article

pubs.acs.org/JPCB

Will It Be Beneficial To Simulate the Antifreeze Proteins at Ice Freezing Condition or at Lower Temperature?

Rajiv K. Kar[†] and Anirban Bhunia*[,†,‡]

[†]Department of Biophysics, Bose Institute, P-1/12, CIT Scheme VII M, Kolkata 700054, India

[‡]Biophysics and Department of Chemistry, University of Michigan, 930 N. University Avenue, Ann Arbor, Michigan 48109, United States

Supporting Information

ABSTRACT: Antifreeze proteins (AFPs) enable the polar living species to survive subzero temperature conditions through effective lowering of the freezing point of body fluids. At the molecular level, AFPs directly interact with the growing seeds of ice crystals to inhibit their formation. To understand the structural and dynamic aspects of this interaction at the atomistic level, molecular dynamics (MD) simulations were carried out on several type I AFPs at multiple temperatures, including the physiologically relevant temperature of 273 K, a lower temperature of 227 K, and the conventional 300 K. A comparison of the principal component analysis (PCA) and mean squared deviation plots for Winter flounder AFP, HPLC6 (mutant of winter flounder AFP), Sculpin, and peptide 1m AFPs reveals that simulations at 273 and 227 K result in the formation of more conserved metastable states than at 300 K. Other parameters such as root-mean-square deviation (rmsd), solvent accessibility surface area (SASA), H-bonding and residual density function (RDF) also suggest the same. MD simulations with ice crystal, where AFPs are complexed to ice plane with TIP4P/ice water model, help in finding relevance of dynamic behavior, and physiological temperature becomes more pronounced. Additionally, a control study on a nonantifreeze protein (LL37) is included, which aids in exploring significant information. On the basis of this approach, it was found that AFPs at 273 and 227 K display relevant dynamic properties that appear at 300 K for nonantifreeze proteins. The present study hence emphasizes the importance of performing computational simulations for antifreeze proteins at the physiologically relevant temperature (273 K), and even at lower temperatures (like 227 K), rather than at room temperatures (300 K).

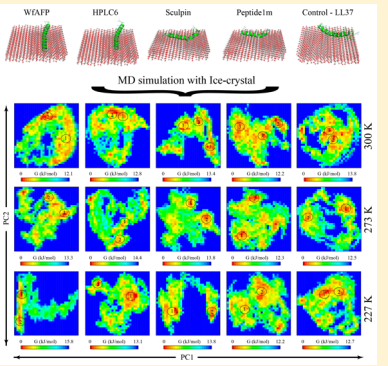

INTRODUCTION

Antifreeze proteins (AFPs) are the key biomolecules that protect the polar species against the challenging subzero climatic conditions. These proteins are produced as a means of adaptation in species such as fish, bacteria, yeast, fungi, plants, and insects by virtue of natural selection.[1,2] The mechanism underlying the physiological role of AFPs relates to lowering the freezing point of water in a noncolligative manner.[3] AFPs, present in blood and other body fluids, bind to the ice surface and prevent further adsorption of ice microcrystals.[4] The mechanism inhibits the crystal layer formation and subsequent ice crystallalization,[5] which is also referred to as the Kelvin effect.[6] Though AFPs have been well studied, the exact mechanism of their ability to bind to ice crystals remains a topic of considerable debate.[7] These studies indicate that residues that are hydrophobic in nature (mainly Ala, Val, and Gly), along with hydrophilic residues like Thr, are responsible for execution of requisite physiological protective role. Hence, there exists a strong relationship between sequential context and structural motif behind the AFP mechanism of action. The selectivity of AFPs binding to the (2021) bipyramidal plane of ice with respect to the crystal growth direction of ⟨0112⟩ has been investigated by Knight and co-workers.[8] It was also postulated that the interatomic distances between Thr residues are crucial for activity when it adsorbed to ice surface.[9] Subsequent investigations disagree with this hypothesis[10,11] and suggest that van der Waals interaction between Asn or Leu to the ice surface drives the binding process.[5] In several other reports, the constrained flexibility of the side chains of hydrophobic residues closer to the binding ice surface[12] suggests an entropy dependent process driving the binding phenomenon.[1,10,13]

To date, AFPs are categorized under five distinct classification types, which are based on sequence, secondary/tertiary structural differences, and their mode of binding to ice crystals.[14] Among these classification types, our group is interested in type I AFPs that are rich in alanine content with α-helical structure.[15] Relevant properties of type I AFPs, such as their small molecular size (3.3−4.5 kDa) and structural simplicity based on α-helices, offer unique excellent platform for engineering of novel antifreeze agents. An example is present in our previous report, where AFPs have been

Received: May 22, 2015
Revised: July 22, 2015

DOI: 10.1021/acs.jpcb.5b04919
J. Phys. Chem. B XXXX, XXX, XXX−XXX

engineered from globular protein *G. antarctica* correlating the antifreeze activity with the helicity and geometrical straightforwardness.[16] In general, the details of biophysical and biochemical properties along with structural studies are usually described using relevant methodologies and techniques. For instance, the structural inference and antifreeze activity conclusion include results from NMR, X-ray, ice recrystallization inhibition assay, and thermal hysteresis. Low-resolution spectroscopy such as circular dichroism (CD) and infrared (IR) spectroscopy is useful in explaining the secondary structure studies. In addition, theoretical studies are much useful in presenting details related to atomistic interaction, dynamicity, contribution of electrostatics, van der Waal forces, and dynamic motional behavior. Taking a keen note to the studies using molecular dynamics simulation for AFPs and non-AFP proteins, the general notation lies in using temperature condition that is close to room temperature (300 K). On the contrary, it is noteworthy to mention that the relevant physiological temperature for AFP functioning is ice-freezing condition (273 K). Thus, the concern lies in relevance and beneficial aspect of using ice-freezing condition instead of room temperature settings for studying AFPs using MD simulations. In the present paper, in addition to the MD-based simulations for AFPs at 300 and 273 K, a lower temperature (227 K) was chosen to fill the existing gap of temperature system in order to understand the atomistic information that describes the mechanism of action of AFPs. Additionally, we were also interested in identifying the structural motif unique to type I AFPs despite their high structural resemblance to straight α helix with antimicrobial peptides such as LL37 (cathelicidins family), which show no antifreeze activity.[16]

METHODS AND COMPUTATION DETAILS

Antifreeze Proteins. Illustrations of the AFPs were carried out with reference to established type I AFPs, viz. Winter flounder AFP (WfAFP) (1WFB.pdb),[17] HPLC6 isoform (1J5B.pdb),[18] Sculpin (1Y03.pdb).[19] In addition to this, recently reported engineered AFP-peptide 1m (2LQ0.pdb)[16] was also included within the scope of this study. WfAFP is a well-recognized antifreeze protein with 37 residues commonly found in Winter flounder fish. HPLC6 is a hydrophobic analogue of WfAFP, where the Thr residues of WfAFP at 2, 13, 24, and 35 were mutated to more hydrophobic Val residues (Thr(2):Val, Thr(13):Val, Thr(24):Val, and Thr(35):Val). Likewise, Sculpin is a 35-residue recombinant form of type I shorthorn Sculpin antifreeze protein possessing a unique discontinuity in its helicity by the presence of a hinge (Ala7 to Thr11) near N-terminal region.[19] Peptide 1m, on the other hand, is a short 25-residue peptide engineered from a globular folded AFP.[16] Notably, these AFPs have a varying range of potency in terms of antifreeze activity, which will be helpful in quantifying the successive results. The dynamic properties of antifreeze peptide were investigated at room temperature (300 K) and at lower freezing conditions of 273 and 227 K.

As a part of control study, a nonantifreeze protein, LL37, is included in the work. It was believed that physiological functioning of type I AFPs is attributed to the geometrical straightforwardness architecture with α-helical structure that can be adsorbed onto ice crystals to retard the crystal growth.[8,14] The said biomolecule is a potent antimicrobial peptide having α-helical structure and antimicrobial activity.[16] Inclusion of control in the study helps in comparing the dynamic behavior in conjunction with the simulation temperature conditions. The present work is divided into two main sections: one is conventional molecular dynamics (MD), and the other is molecular dynamics with ice crystal, the details of which are provided in the preceding section. The convention MD was carried out with commonly used water molecules (TIP3P water models). It is widely known that room temperature conditions with TIP3P water models are accurate in terms of calculation of biophysical or biochemical properties of proteins, DNA, and RNA. The same is also true with other relevant water models like SPC and TIP4P. Although there are many theoretical studies for AFPs that are based on this conventional MD approach, there exists a limitation in terms of force-field parameters. The reason is associated with the fact that AFPs are physiologically relevant with ice-freezing temperature,[20−22] which infers that using the water model containing TIP4P/ice model is more appropriate compared to TIP3P model.[23−25] For comparison purposes, we have used the nonantifreeze protein LL37 as a control.[16] To the best of our knowledge, a comparative study of nonantifreeze protein using TIP4P/Ice model with typical AFPs has not been reported in the literature.

Conventional Molecular Dynamics. All computational simulations were carried out in Amber11 and Amber14 suite of programs using ff99SB force field[26] on a GPU workstation having C600/X series Tesla card.[27] Each peptide was solvated in a truncated octahedron box of 10 Å edge dimension containing TIP3P water models.[28] All the charges in the system were neutralized by the addition of appropriate number of counterions. Electrostatic interactions were calculated using PME method with cubic β-spline interpolation and a grid spacing of 1 Å. The nonbonded cutoff was kept at 1.0 nm for both Coulomb and Lennard-Jones interactions. The MD integration time step was 2 fs. Reordering of hydrogen bond lengths was constrained through SHAKE algorithm with a relative tolerance value of 10^{-5} Å.[29] Periodic boundary conditions (PBC) were employed in each system in the three-dimensional space, and a uniform density approximation was made to retain correct van der Waals interactions.[30]

Molecular Dynamics with Ice Crystal. All procedures described in the previous section were precisely followed in conjunction with ice crystals. Importantly, the use of control nonantifreeze protein LL37 (2K6O.pdb) was also studied with ice crystal plane.[31] The bipyramidal (2021) ice crystal planes have a crystal growth direction of ⟨0112⟩. Preparation of theoretical model of ice crystal was built using a model collected from Dalal et al.[32] The complex of AFPs as well as with the control peptide LL37 with ice crystal was prepared using Hex software[33] (Figure S1 in Supporting Information). Next, the complexes were solvated in Amber using tleep module. All water molecules (ice crystal and solvation water) were parametrized using TIP4P/ice water models.[34] The parameters for solute atoms were in accordance with ff99SB force field.[35] The protocol for energy minimization of the system and heating steps was adopted from a published report by Calvaresi et al.[36] In brief, the solute molecules experience gradual increase in temperature with and without weak restraint of 1 (kcal·mol^{-1}) Å^2. Isotropic position scaling (switching from *NVT* to *NPT* microcanonical ensemble) and vice versa were approached during the heating steps.[36] Other relevant parameters, including physical integration steps and pressure scaling system, were similar to those of conventional MD simulation. A production run in specialized MD simulation was

DOI: 10.1021/acs.jpcb.5b04919
J. Phys. Chem. B XXXX, XXX, XXX−XXX

continued for a time period of 25 ns, and the trajectory frames were saved at an interval of 4 ps for analysis.

Principal Component Analysis. Principal component analysis (PCA) is used to explore the correlated motions in solute atoms represented by large number of degrees of freedom.[37] This is also known as essential dynamics, where key variables involved in governing the motion can be pointed in relevance.[38] The conformation sampling data in higher dimensions when projected onto few principal components reduce the dimensionality of the data.[38,39] In the present technique, the symmetrical covariance matrix **C** constructed from the atomic coordinates was diagonalized with an orthonormal matrix **R**. Mathematically, this can be represented as $\mathbf{R}^T\mathbf{CR} = \mathrm{Diag}(\lambda)$, where λ represents the eigenvalues such that $\lambda_1 > \lambda_2 > ... > \lambda_n$. Each of the eigenvalues will be associated with an eigenvector **R**, which is also known as the essential modes or principal modes.[38] Furthermore, the orthonormal transformation represents the data in a new coordinate system whose directionality is defined by the eigenvectors **R**. Notably, the projection of the simulation trajectory over the principal modes is referred to as scores of the principal components (PCs). In our current PCA analysis, the globular rotational and translational motions of AFPs were excluded so that only the internal motions can contribute. This sort of filtering is performed through least-squares fitting to a frame of reference for all atoms in AFPs or selectively Cα atoms. The obtained eigenvalues ($\lambda_1, \lambda_2, ..., \lambda_n$) represent the mean square fluctuation or variance in global motions for each principal component, 1 to n, respectively. The cosine content of the PCs is calculated using eq 1:

$$\text{cosine content} = \frac{2}{T}\left(\int_0^T \cos(i\pi t/T)\, p_i(t)\, \mathrm{d}t\right)^2 \left(\int_0^T p_i^2(t)\, \mathrm{d}t\right)^{-1} \quad (1)$$

It is well recognized that the PCs of random diffusion are cosine with respect to the number of periods half of that of the PC index.[39] PC index (PC_i) is proportional to the inverse of the square root of the eigenvalue ($(\lambda_i^{-1})^{1/2}$). The cosine content can take a value between 0 and 1 depending on whether the shape represents a perfect cosine shape or other shapes, respectively.[39] If the cosine contents of first few PCs were close to 1, then the major contributions to root mean squared fluctuations are due to random diffusion rather than any variations in potential. The module "g_covar" built in GROMACS, version 4.0.5, was used for the covariance matrix calculation.[40] PCs for all atoms and selective Cα atoms of AFPs at all temperature conditions were calculated from the simulation trajectories using the "g_anaeig" module. Only the first two PC components were used in the PCA analysis for all AFP systems. Average structures of the AFPs corresponding to PCs were extracted using PCAsuite (http://mmb.pcb.ub.edu/software/pcasuite/). Porcupine plots for the visual representation of motional fluctuations were prepared using a Perl script.[41]

Mean Squared Displacement Calculation. The displacement of solute atoms in solution always follows a path of random collision. This enables the simulation of the trajectories followed by the complex conformations of the associated system within the three-dimensional space.[42] Because of the stochastic nature of conformational state sampling, each sequential step in the trajectory is independent of its previous step.[43] Thus, mean squared displacement (MSD) represents the thermal displacement of each atom from its averaged center of mass. MSD for a simulated trajectory is calculated[44] using eq 2:

$$\begin{aligned}\mathrm{MSD}(t) &= \langle |r(t) - r_{\mathrm{cm}}(t)|^2 \rangle \\ &= \langle |[r_i(t) - r_i(0)] - [r_{\mathrm{cm}}(t) - r_{\mathrm{cm}}(0)]|^2 \rangle \end{aligned} \quad (2)$$

where $r_i(t)$ denotes the position of atom i at time t, cm represents the center of mass, and $\langle\rangle$ represents the average. MSD can also be calculated from the first two PCs obtained from essential dynamics. Since the first two PCs contribute to more than 70% of the motional fluctuations in the simulation trajectory, MSD calculated from principal components can provide crucial information on global dynamics.[42] Eigenvalues of PC1 and PC2 were obtained for all atoms, main-chain atoms, side-chain atoms, and Cα atoms in AFPs to calculate the MSD using "g_msd" module of GROMACS.

Thermodynamics Parameters. The energy landscapes pertaining to the conformational space of PCs (PC1 and PC2) were computed using the "g_sham" module of GROMACS according to eq 3:[45]

$$v_i = k_b T \ln\left[\frac{P(xi)}{P_{\max}(x)}\right]^2 \quad (3)$$

where k_b is the Boltzmann constant, T is the temperature which can be either 300 or 273 K according to the trajectory considered, $P(xi)$ is the estimate of the probability function, and $P_{\max}(x)$ is the probability of the most probable state.[46] The remaining analyses presented in this study were computed using "ptraj" and "cpptraj" module of Amber. The hydrogen bond occupancies were computed using Hbonanza software[47] and VMD modules[48] with cutoff values of 3 Å and 35° for distances and angles, respectively. Free energy basin analysis was performed using Wordom software. In this analysis, "tau-commit" represents the microstate of each basin, and "p-commit" represents those microstates whose probability is ≥0.5. VMD is used for the preparation of porcupine plots projection.[49]

RESULTS AND DISCUSSION

System Optimization of AFPs in Conventional MD Simulation. The binding profile of AFP at higher concentration orients to either the prism plane [1 0 −1 0] or the secondary prism plane [1 1 −2 0]. On the other hand, the conservative binding behavior of AFPs occurs in the direction of ⟨−1 1 0 −2⟩ with reference to the bipyramidal plane of hexagonal ice crystals.[8] It is important to mention that there is no clear evidence available that sheds light on the binding process and temperature of AFPs with ice crystals. In this regard, it would be appropriate to state that the present study focuses on fulfilling the gap by exploring the relevance of temperature system used in MD simulation for AFPs. The said assumption is thus brought into comparison with a broader temperature window of room temperature (300 K), ice-freezing condition (273 K), and further lower temperature condition (227 K). The importance of temperature condition in MD simulation is dictated with the help of kinetic velocity, which is converted by the heat of the system. This can be understood by realizing that the dynamics under Newtonian law of motion have difficulty in maintaining the intramolecular distance

DOI: 10.1021/acs.jpcb.5b04919
J. Phys. Chem. B XXXX, XXX, XXX−XXX

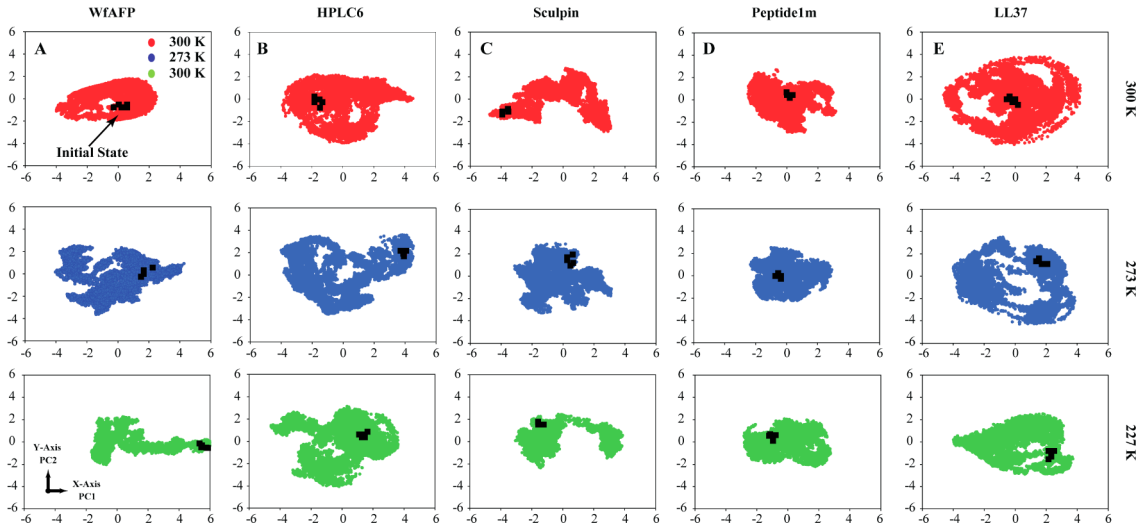

Figure 1. Correlated projection of PC1 and PC2 for AFPs obtained by MD simulations with ice crystal. The projections of 300, 273, and 227 K are shown in red (upper panel), blue (middle panel), and green (lower panel) contours, respectively. Contour plots represent PCA for (A) WfAFP, (B) HPLC6, (C) Sculpin, (D) peptide 1m, and (E) LL37.

constraints between the O and H atoms of water molecules. In contrast, the kinetic velocity of the atoms for the desired equilibrium temperature is well preserved during simulation. This indicates that the adoption of temperature system in MD simulation maintains the approximation of corresponding physiological temperature. Initial assumption for system optimization was performed for simulation systems with TIP3P water models. The details were carried out for kinetic energy, potential energy, and their corresponding root mean squared (rms) values (Table S1 in Supporting Information).

Globular Dynamics of AFPs. The first two PCs, viz. PC1 and PC2, account for more than 70% of fluctuations with a minimum degree of freedom less than 1%.[38] Cosine content is the crucial indicators, which have potential to dictate the convergence criteria in PC analysis.[50] The cosine contents for these PCs were calculated and are summarized in Table 2 and Table S2 (Supporting Information). The cosine content of PC1 for all systems at 300 and 273 K was <0.5, suggesting sufficient sampling and minimum contributions from random diffusion. On the other hand, some of the PC1 components for WfAFP, Sculpin, and peptide 1m at 227 K showed insufficient sampling with cosine content of >50%. The cosine content of PC2 to PC1 suggests a higher degree of sampling with sufficient shuffling for the trajectories. In general, the convergence of the rmsd factor will be meaningful when the initial time period of the simulation is excluded from the analysis. The computed cosine content for the second half (13−25 ns) reflects more stability and minimum fluctuation in conjunction with random diffusion. A meaningful and precise inference is further achieved considering only the Cα atoms for the said trajectory portion, which represents sufficient conformation sampling.

Behavior of AFPs Analyzed in MD Simulation with Ice Crystal. Specific attributes of antifreeze activity in conjunction with local melting of ice have been precisely defined by Calvaresi et al.[36] It has been reported that ice crystal melts (loss of relative restraints of water molecules) even at below freezing temperature (260 K) at approximately 10 ns time scale. Similar observation is revealed in our simulation, where ice melts at approximately 10 ns. Calvaresi et al.[36] also revealed that the loss of restraints among water molecules occurred below the ice-freezing condition (260 K) even in the presence of AFPs. This in other terms is being referred to melting of ice, in conjunction with the virtual computational modeling. Information pertaining to use of 300 K temperature system for proteins is well-known, which generates our interest in exploring the dynamic pattern of proteins at lower temperature. In order to demonstrate the accuracy of the computational methodology of the previous section, a similar analysis is carried out with the results of our specialized MD simulation.

Principal component analysis (PCA) for protein conformation reveals unique behavior in specialized MD simulation, which can be attributed to the presence of ice. The conformational space spanned by AFPs at 300 K is conserved (Figure 1). For better visual inspection, the axis scale was fixed for all scatter plot representations. The correlated projection of PC1 and PC2 at 273 K for AFPs shows that protein conformation attains a sufficient degree of freedom. These data are close to the realistic condition, as AFPs in the presence of ice reflect its physiological relevance. A conventional scattering of PCA projection contours especially for WfAFP, HPLC6, and Sculpin is found at 273 K as well as 227 K. Projections of PC1 and PC2 in wfAFP at 273 K completely differ from those at 300 K, where the data points are more diffused (Figure 1A). As expected, the melting time of ice in our simulation corresponds to the system temperature. The projection at 227 K also differs, which might be attributed to adherence with ice crystal at this temperature. Similar pattern is observed in the cases of HPLC6 and Sculpin (Figure 1B and Figure 1C), which is realized as characteristic projection for dynamicity of AFPs with ice crystal. The dynamic behavior of peptide 1m is almost comparable at all temperature scales and it was realized that such conduct of dynamicity is linked with antifreeze property of these AFPs (Figure 1D). Note that the antifreeze property of peptide 1m is approximately 50- to 100-fold less compared to typical AFPs.[16] On the contrary, similar trend is observed for control peptide (LL37) at all temperature conditions, where any deviation is attributed to temperature difference over the complete system and is not attributed to functional aspect of protein. Typically, the PCA projections for LL37 remain unchanged for 300 and 273 K. This is reflective with realistic projection pattern (Figure 1E), which is indicative of attenuation for sufficient dynamicity. Details of PCA with

DOI: 10.1021/acs.jpcb.5b04919
J. Phys. Chem. B XXXX, XXX, XXX−XXX

respect to conventional MD simulation are provided in Figure S2 of the Supporting Information.

Diffusion Characteristics of AFPs. Estimation of the diffusive characteristics of AFPs analyzed by mean squared displacement (MSD)[51] along PC1 and PC2 showed a marked difference (Figure 2A–D) at all temperature conditions for all

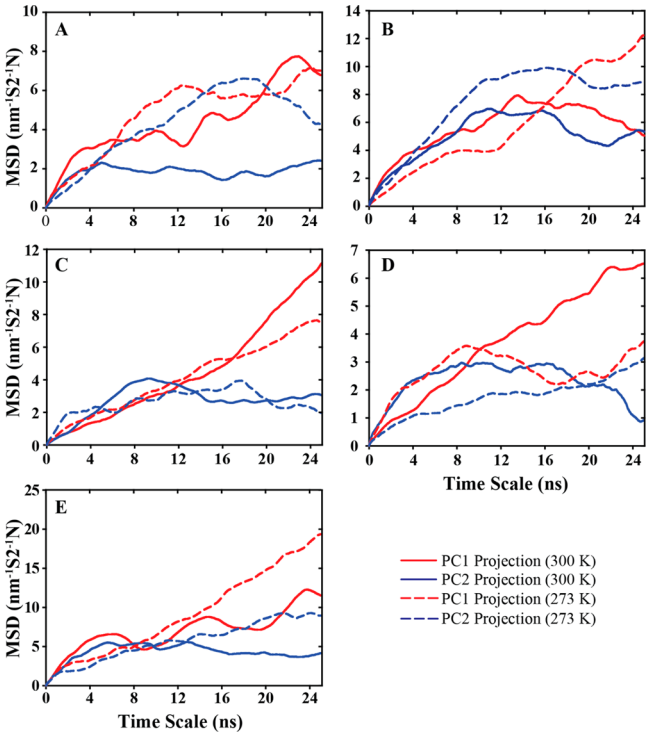

Figure 2. Mean square deviation analysis of projection from PC1 and PC2 of MD simulations with ice crystal for (A) WfAFP, (B) HPLC6, (C) Sculpin, (D) peptide 1m, and (E) LL37.

AFPs elucidated from MD simulation with ice crystal. The details of diffusion characteristics obtained using conventional MD simulation are provided in Supporting Information (Figures S3, S4, and S5). The MSD along the PC1 projection for trajectory at 300 K showed no convergence for Sculpin and peptide 1m, indicating that trajectory follows a Brownian motion with high cosine content (Table 1). Trajectories of the remaining systems were found to be well conserved in the period of 60–80 ns, except for LL37, which shows higher scale of Brownian motion. Such convergence demonstrates that near 12–16 ns time scale, the random diffusion of these AFPs has completely disappeared, and the conformations encountered a potential energy barrier in its free energy landscape. The MSD along PC1 at 273 K for HPLC6 and control peptide LL37 did not show any convergence (Figure 2C and Figure 2E). This is an indication that the order of displacement varies with 2-fold magnitude and that a strong Brownian motion in the trajectory is observed. In contrast, the MSD along PC2 for trajectories at 300 and 273 K showed higher convergence for all AFPs. Time profile of MSDs at 273 K for all systems except peptide 1m was linear up to 5 ns. Notably, the convergence of MSD due to diffusion is also conserved for WfAFP, HPLC6, and peptide 1m approximately at 8 ns, whereas the same convergence is seen at 16 ns for Sculpin.

Disappearing of random diffusion is found at 8 ns in all cases, which suggests that the subdiffusive motions encounter a strong potential energy barrier.[51] The MSD plot depicting the thermal fluctuation of atomic displacement from the average position is shown in Figure 3. Note that these fluctuations are references to the center of mass, which reveals that better convergence criteria are achieved. The differences in MSD calculated by the two approaches are due to the presence of large number of degrees of freedom for all-atom analysis compared to PC-based analysis. MSD provides information on diffusion property of solutes, which tends to increase rapidly with increase in temperature.[51] MSD at 300 K accounts for increased external protein diffusion (rotational and translational motions) and internal protein diffusion (anharmonic motions). The extent of diffusion by means of rotational, translational, and anharmonic motions is observed in MSD of various atoms under consideration for all AFPs at 300 K (Figure 3 and Supporting Information Figure S6). MSD plot represents the motion of AFPs accroding to the antifreeze activity potential of molecules. The pattern for internal and external motion of WfAFP and HPLC6 differs from that of Sculpin and peptide 1m, which are less potent in terms of antifreeze activity. In the cases of WfAFP and HPLC6, the diffusion seems to be higher at 273 K, whereas in control peptide, diffusion at 300 K dominates. These data indicate that temperature conditions are crucial in determining the physical properties of antifreeze biomolecules at virtual system. Interestingly, the diffusion properties for all AFPs are precise at 273 K in comparison to 300 K, when analyzed from MD simulation with ice crystal (Figure 3 and Supporting Information Figure S6). Similar pattern is also observed at 227 K (Supporting Information). Particularly, the side chain diffusion pattern for all AFPs is more prominent at low temperature of 227 K than 300 K. These data indicate that the water trapping times in local minima across the potential surface of ice crystal is higher at lower temperature for AFPs. On the contrary, it can be found that the diffusive behavior of the control peptide LL37 is optimum at 300 K for its side chain. These data suggest that diffusion of internal protein motion (rotational and translational) and external protein motion (anharmonic motions) for LL37 is precise at 300 K, where the same for AFPs is precise at 227 K. MSDs for AFPs at 227 K are given in Supporting Information (Figures S7 and S8).

The rmsd plot complements the MSD analysis by accounting for conformational flexibility or stability during the course of the simulation (Supporting Information Figure S9). Interestingly, a comparison of the rmsd and MSD profiles at various temperature conditions shows that the conformations were stable in the following order 227 K > 273 K > 300 K.

Residue Specific Analysis of AFPs Conformation. The rmsd (Supporting Information Figure S9) of AFPs indicates that the peptides fluctuate significantly at 300 K, whereas they become rigid at 273 K and more precise at 227 K. This agrees with the fact that at lower temperatures the entropy of the solute system decreases. In fact, the decrease in entropy is desired over fluctuating side chains for the adsorption of AFPs to the ice surface. We also observe a marked difference in the fluctuating behavior of individual residues of WfAFP. In particular, continuous stretches of Ala residues from Ala6-Ala11 and Ala28-Ala34 show an equitable fluctuation at 273 and 227 K, whereas the same stretches of amino acids were more flexible at 300 K, as depicted by RMSF plots (Figure 4). A comparative plot for RMSF calculation from conventional MD simulation is provided in Supporting Information (Figure S10). This is in accordance with the hypothesis that the least dynamic hydrophobic residues play an important role in ice binding.

DOI: 10.1021/acs.jpcb.5b04919
J. Phys. Chem. B XXXX, XXX, XXX–XXX

Table 1. Cosine Content on the Principal Component (PC1 and PC2) from Normal Room Temperature and Ice Freezing Condition Simulation of Antifreeze Peptides

	cosine content (300 K)		cosine content (273 K)		cosine content (227 K)	
AFP	PC1	PC2	PC1	PC2	PC1	PC2
Winter flounder	0.005[a]	0.006[a]	0.449[a]	0.022[a]	0.669[a]	0.062[a]
	0.027[b]	0.037[b]	0.062[b]	0.854[b]	0.083[b]	0.438[b]
	0.004[c]	0.001[c]	0.344[c]	0.147[c]	0.624[c]	0.223[c]
	0.072[d]	0.022[d]	0.193[d]	0.653[d]	0.067[d]	0.440[d]
HPLC6	0.450[a]	0.031[a]	0.316[a]	0.017[a]	0.004[a]	0.000[a]
	0.054[b]	0.059[b]	0.145[b]	0.872[b]	0.002[b]	0.312[b]
	0.400[c]	0.018[c]	0.274[c]	0.092[c]	0.000[c]	0.002[c]
	0.068[d]	0.156[d]	0.420[d]	0.750[d]	0.009[d]	0.509[d]
Sculpin	0.178[a]	0.890[a]	0.000[a]	0.514[a]	0.047[a]	0.245[a]
	0.028[b]	0.362[b]	0.142[b]	0.065[b]	0.656[b]	0.043[b]
	0.261[c]	0.819[c]	0.152[c]	0.416[c]	0.049[c]	0.146[c]
	0.022[d]	0.112[d]	0.000[d]	0.399[d]	0.646[d]	0.039[d]
peptide 1m	0.033[a]	0.006[a]	0.204[a]	0.001[a]	0.406[a]	0.263[a]
	0.004[b]	0.002[b]	0.010[b]	0.186[b]	0.502[b]	0.406[b]
	0.051[c]	0.018[c]	0.142[c]	0.029[c]	0.358[c]	0.302[c]
	0.031[d]	0.012[d]	0.177[d]	0.385[d]	0.412[d]	0.428[d]
LL37	0.161[a]	0.001[a]	0.030[a]	0.488[a]	0.358[a]	0.220[a]
	0.046[b]	0.035[b]	0.143[b]	0.274[b]	0.232[b]	0.020[b]
	0.052[c]	0.089[c]	0.014[c]	0.649[c]	0.225[c]	0.469[c]
	0.148[d]	0.000[d]	0.008[d]	0.425[d]	0.309[d]	0.031[d]

[a]Attributes to cosine content from PC computed for all atoms for 0−13 ns. [b]13−25 ns. [c]Attributes to cosine content from PC computed for Cα atoms for 0−13 ns. [d]13−25 ns.

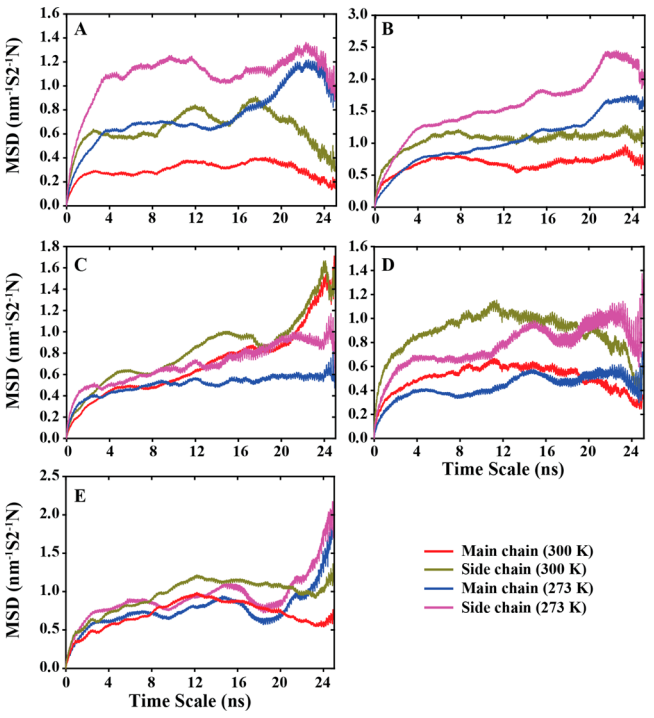

Figure 3. Account of the mean-squared displacement of side chain atoms and main chain atoms obtained by MD with ice crystal for (A) WfAFP, (B) HPLC6, (C) Sculpin, (D) peptide 1m, and (E) LL37.

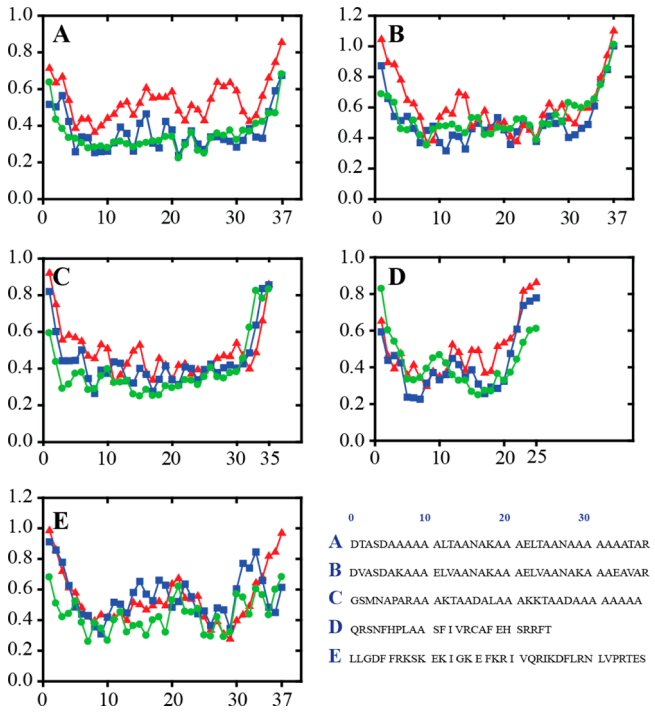

Figure 4. Root-mean-squared fluctuation of amino acids extracted from simulated trajectory with ice crystal for (A) WfAFP, (B) HPLC6, (C) Sculpin, (D) peptide 1m, and (E) LL37. Color codes used depict system behavior at 300 K (red), 273 K (blue), and 22 K (green). The amino acid sequences of all AFPs are shown at the bottom.

Similar behavior was observed for HPLC6 at 273 K as well as 227 K when compared with 300 K. The fluctuations near terminal residues for all AFPs were significantly higher compared to the rest of the residues at both temperatures. Sculpin, whose contagious stretches of Ala residues are present near C-terminal region (Ala28-Ala35), was found to be highly fluctuating under both conditions. Overall, it suggests that positioning of the Ala residues near the terminal region is least preferred if enhanced antifreeze activity is desired.

An animated depiction of the motional fluctuations can be represented in porcupine plots, where the displacement

DOI: 10.1021/acs.jpcb.5b04919
J. Phys. Chem. B XXXX, XXX, XXX−XXX

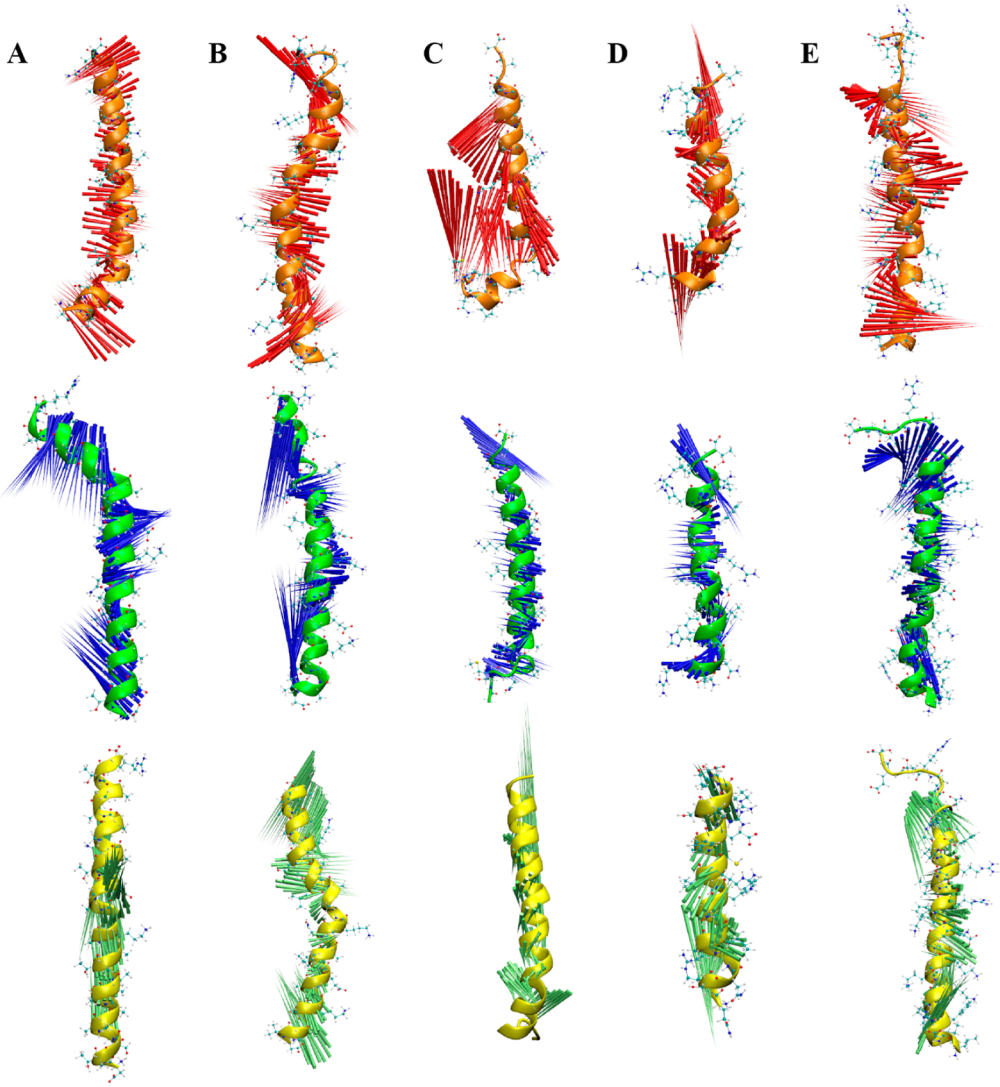

Figure 5. Porcupine plots showing the projection of PC1. Red color porcupine plots (upper panel) depict the system at 300 K. The blue color porcupine plots (middle panel) depict the system at 273 K, and the green color porcupine plots (lower panel) depict the system at 227 K. Representation models correspond to (A) WfAFP, (B) HPLC6, (C) Sculpin, (D) peptide 1m, and (E) LL37.

between the average coordinates of Cα atoms and the most deviated conformation can be represented through vectors with the respective average coordinates of backbone atoms as the origin (Figure 5). The motional fluctuations of WfAFP seem to be more ordered at 273 K compared to 227 and 300 K. It is also clear that the continuous stretches of hydrophobic residues like Ala6-Ala11 and Ala19-Ala21 tend to move toward Leu12 and Leu23 to make the hydrophobic contacts. Similar to WfAFP, HPLC6 also exhibits higher motional fluctuations at 300 K relative to 273 and 227 K, but a form of scissoring movements directs the hydrophobic contacts (Figure 5B). In peptide 1m, significant motional fluctuations are observed at all temperature conditions, with the helical content strongly perturbed particularly at 300 K. A similar analysis was carried out with respect to conventional MD simulation and is given in Supporting Information (Figure S11).

Thermodynamic Profile Analysis. Features observed from the heat maps of the energy landscape indicate that larger population of conformations have higher energy at 273 and 227 K (green to blue) compared to 300 K (red to green) (Figure 6A–E). On the contrary, an opposite pattern was found in the case of MD simulations with TIP3P water models (Supporting Information Figure S12). It indicates that thermodynamically more stable conformations can be elucidated at 273 K than at 300 K. The difference in the energy gap in terms of individual scale of Gibbs free energy is also higher compared to 273 and 227 K state. We found two metastable transient states for WfAFP and HPLC6 in the probability sampling energy landscape (Figure 6A,B) at the trajectories. Notably, the helicity of HPLC6 was always perturbed over an extended period in the simulation (8–12 ns). Such helical perturbations have a precise role in overcoming the potential energy barrier to achieve a minimum for the conformations. In the case of Sculpin, we have identified more than two transient metastable states from the energy landscape (Figure 6C and Figure 6D) at 300 K, but only two such metastable states were found from the trajectory at 273 K. There exists certain difficulty in elucidating the correct time point at which these transient states originated in the trajectory at 273 K because most of these conformations looked similar. For the simplicity of analysis, we have made a rough estimation of 2D cluster based on rmsd of conformation. Details of

DOI: 10.1021/acs.jpcb.5b04919
J. Phys. Chem. B XXXX, XXX, XXX–XXX

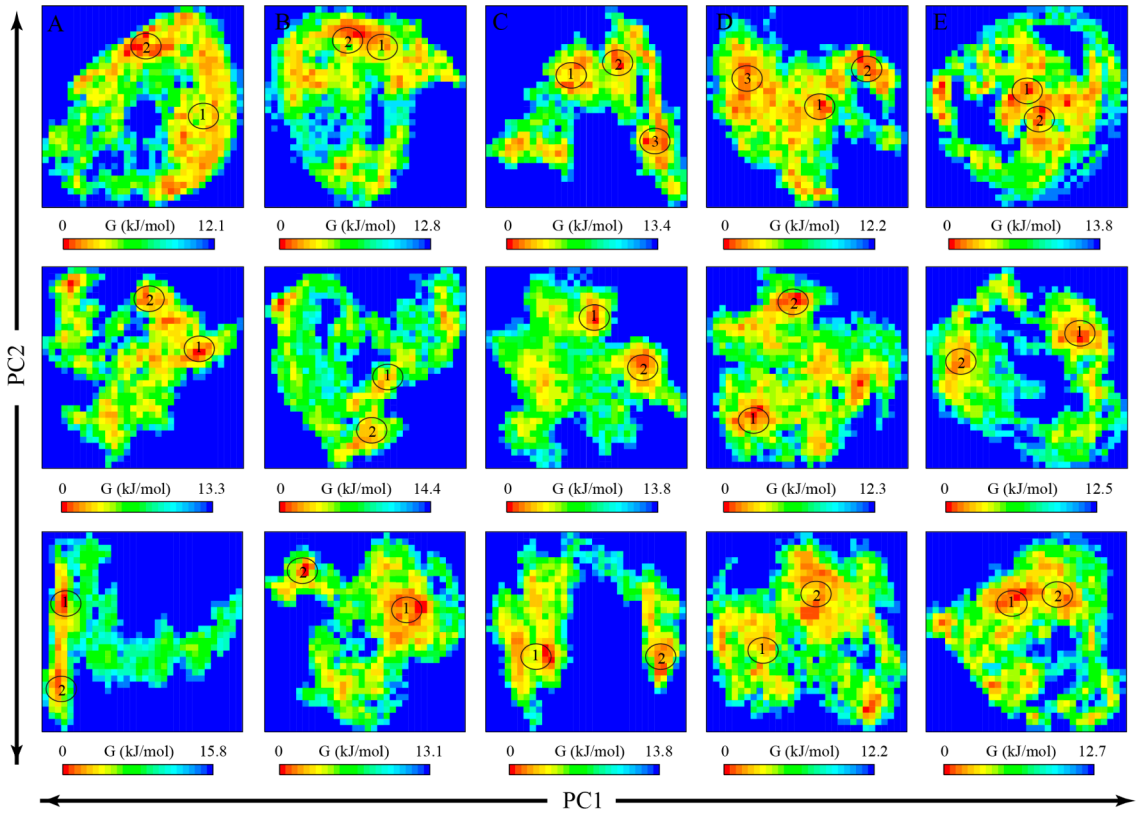

Figure 6. Energy landscape with respect to the sampling probability of occurrence of any transient state conformations obtained by MD with ice crystal. The energy scale of individual landscape plots has been shown for WfAFP (A), HPLC6 (B), Sculpin (C), peptide 1m (D), and LL37 (E). The upper, middle, and lower panels correspond to results obtained from simulations at 300, 273, and 227 K, respectively. The presence of any transient state in the conformational sampling is highlighted by a circle.

clusters for AFPs and control LL37 are provided in Supporting Information (Figure S13). From the energy landscape, it can be revealed that the probability of finding similar states appears to be diffused throughout the region. In the case of peptide 1m, three transient states were present at 300 K, while only two metastable states were identified at 273 K (Figure 6D and Figure 6I). The helicity of peptide 1m was found to be more perturbed leading to a greater degree of loss in geometrical straightforwardness at 300 K compared to 273 K, which is also evidenced from the porcupin plots. Peptide 1m has a close approximation in the energy state of conformations, which is in accordance to lower antifreeze activity with reference to other three AFPs. Interestingly, the results corresponding to the control peptide LL37 completely disagree with the above-described trend. The energy states of conformations are more at higher energy state (green to blue) at 300 K and at lower energy state (red to green) at 273 K. The difference in energy state for LL37 can also be attributed to the area coverage by the data points in conformation space at 300 K compared to 273 K.

Hydrogen-Bonding Pattern. Radial distribution function (RDF) is a measure of the density of solvent molecules adjacent to the surface of solute molecules. The density of water molecules near the surface of AFPs is not differing up to a distance of 2.75 Å at all temperature conditions. The average density obtained through integration yields a value of 1.5. Comparison of the water molecules near the AFPs at a distance of 4 Å was ∼9.06 at 300 K and 8.70−9.86 at 273 and 227 K, respectively. Furthermore, the average number of water molecules increased with an increase in the separation distance as evidenced in all AFPs except for control LL37. Such efficient packing of solvent molecules (Figure 7A−C) around WfAFP, HPLC6, and Sculpin, at 273 and 227 K, explains why these molecules exhibited a reduced fluctuation during the course of the simulation. Note that this diffrence also persists between 273 and 227 K. In addition, the higher density of solvent reduces the fluctuation to an extent that the hydrophobic residues of AFPs can efficiently adsorb to the surface of the ice plane. This can be easily verified for peptide 1m (Figure 7D), the AFP with the least number of hydrophobic residues considered here. In the case of peptide 1m, we find the number of water molecules at 4 Å to be 9.1, 8.8, and 8.9 at 300, 273, and 227 K, respectively. With an increase in separation distance, e.g., 8−9 Å, the water packing at 300 K was similar to that of 273 K, as in the case of non-AFP LL37 (Figure 7E). Overall, the solvent-accessible surface area (SASA) for all AFPs was found to differ at 300 K compared to 273 K and lower temperature, most likely due to increased fluctuations. The results from RDF and SASA analysis thus provide new insights into the mechanistic details of the interaction between AFPs and water molecules at lower temperature conditions. A similar trend of integrated water molecule numbers for AFPs is found with conventional MD simulation (Supporting Information Figure S14). The packing of water molecules at both temperature systems is comparable.

Kelvin Effect. MD simulations carried out at different temperature conditions suggest entropic favorable binding of AFPs near the ice binding plane.[52,53] From the results of radial distribution function, no significant changes have been witnessed for any of the simulation conditions. This also implies that there is a negligible change in terms of H-bond

DOI: 10.1021/acs.jpcb.5b04919
J. Phys. Chem. B XXXX, XXX, XXX−XXX

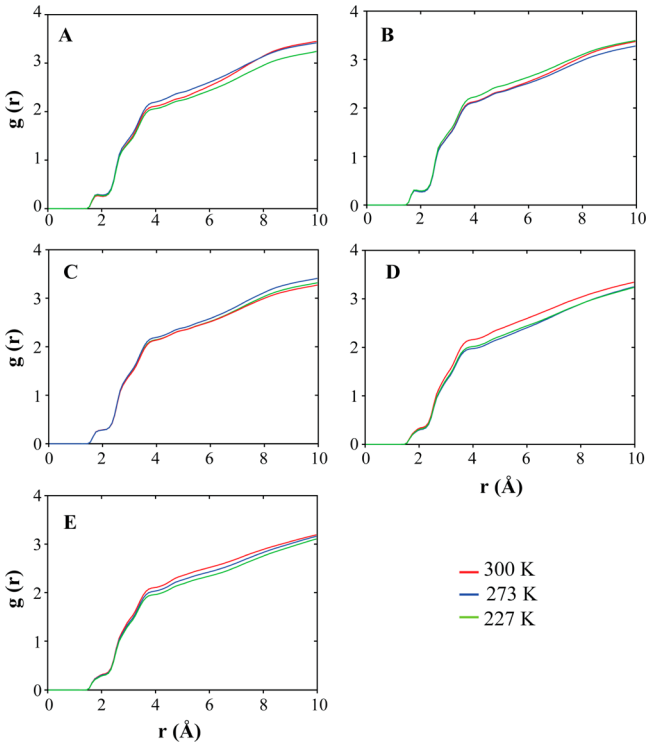

Figure 7. Plot showing the distribution of solvent molecules over surface of AFPs by means of radial distribution function: (A) WfAFP; (B) HPLC6; (C) Sculpin; (D) peptide 1m; (E) LL37.

formation between water molecules and solute protein molecules. Thus, we conclude that the local hydrogen-bonding network does not play a significant role in governing antifreeze activity. However, the stability of ice crystal varies as presumed in conjunction with the temperature system.[54] If k_{melt} denotes the rate of ice crystal melting, then k_{melt} follows the order of 300 K > 273 K > 227 K. We also observed that the changes in secondary structure for AFPs are minimum in the case of hydrophobic residues compared to the hydrophilic residues. This fluctuation also varies according to the temperature system as evidenced from RMSF plots. Notably, the ice melting behavior in the presence of LL37 is more pronounced compared to that of AFPs. Ice melting in the presence of LL37 starts at ∼2 ns when simulation was performed at 273 K, in comparison to <3 ns at 227 K. Similar behavior was also observed in the case of peptide 1m where ice crystals do not last for more than 3−4 ns time period. A remarkable difference was observed in the cases of WfAFP and HPLC6, where the melting happens at approximately 2 ns, >6 ns, and >8 ns time scale at 300, 273, and 227 K, respectively. These results can be well correlated with corresponding antifreeze potential of these biomolecules.[36] We also observed that the melting of water molecules along with the liquid water tends to oppose a thrust on AFPs, which prevents drifting away of AFPs from the ice crystals. Overall, these results, in conjunction with the k_{melt} and behavior of control peptide LL37, explain the Kelvin effect.

CONCLUSION

In summary, the present study emphasizes the significance of performing MD simulation of antifreeze proteins at the physiologically relevant temperature of 273 K and ice freezing temperature of 227 K rather than at 300 K. Studying the dynamics of biological molecules through principal component (PC) based analysis and free energy evaluations provides mechanistic insights at the atomic level.[55] Application of conventional MD simulations at 300 K and replica exchange molecular dynamics at a varying temperature are some of the commonly adopted approaches for studying AFPs.[56,57] However, it is quintessential to perform simulations at the physiologically relevant temperature, e.g., 273 or 227 K, in order to fully understand the molecular mechanism of AFP binding to ice and inhibition of crystal growth.[4,8,10] Herein, we have focused on profiling the dynamics and flexibility of the well-known AFPs such as WfAFP, HPLC6, Sculpin, and peptide 1m at temperature conditions of 300 and 273 K using TIP3P water model as conventional MD simulation. Furthermore, MD simulations were carried out for AFP−ice complex using TIP4P/ice water model with inclusion of control nonantifreeze peptide (LL37). On the basis of the essential dynamics and MSD analysis for all AFPs, we have found that molecular motions are well conserved at ice-freezing conditions (273 and 227 K) compared to room temperature (300 K). Using MD simulations, in which the AFPs are complexed to ice plane with TIP4P/Ice water model, it becomes notably evident that at lower temperature conditions, the AFPs exhibit relevant dynamic properties that appear at 300 K for non-AFP proteins. We have also found that among all AFPs considered, WfAFP shows a maximum difference in per residue fluctuation when compared at the three different temperatures, whereas peptide 1m shows the minimum difference. On the basis of RDF and SASA analysis, our results suggest that the crowding and ordering of water molecules at lower temperature (such as 273 and 227 K) in the vicinity of the solute surface facilitate the adsorpotion of contiguous stretches of Ala residues to ice through hydrophobic interaction. Finally, the smaller spread in the energy landscape profile and free energy profile allowed us to conclude that the overall energy estimates of the AFPs are more stable at lower temperature than at 300 K.

ASSOCIATED CONTENT

Supporting Information

The Supporting Information is available free of charge on the ACS Publications website at DOI: 10.1021/acs.jpcb.5b04919.

Ice lattice model used for the MD simulation (Figure S1); information related to conventional MD simulations with TIP3P water models (Tables S1 and S2, Figures S2−S6, S10−S14); MSD for AFPs at 227 K (Figures S7 and S8); and rmsd plots (Figure S9) (PDF)

AUTHOR INFORMATION

Corresponding Author

*E-mail: bhunia@jcbose.ac.in or abhunia@umich.edu.

Notes

The authors declare no competing financial interest.

ACKNOWLEDGMENTS

The research was supported by Council of Scientific and Industrial Research (CSIR) (Grant 02(0005)/11/EMR-II), Government of India. A.B. thanks Dr. Samuel A. Kotler (University of Michigan) and Dr. K. Janarthanan (Vclinbio Pvt. Ltd., India) for critical reading and editing of this manuscript. We are grateful to Drs. Subhrangsu Chatterjee and Debjani Roy (Bose Institute, Kolkata, India) for allowing us to use AMBER14 software suite and GPU workstation, respectively. R.K.K. thanks CSIR, Government of India, for Senior Research

DOI: 10.1021/acs.jpcb.5b04919
J. Phys. Chem. B XXXX, XXX, XXX−XXX

Fellowship (SRF) (Grant 09/015(0467)/2014-EMR-I). We thank three anonymous referees for their valuable suggestions to improve the quality of the manuscript.

REFERENCES

(1) Chao, H.; Houston, M. E.; Hodges, R. S.; Kay, C. M.; Sykes, B. D.; Loewen, M. C.; Davies, P. L.; Sönnichsen, F. D. A diminished role for hydrogen bonds in antifreeze protein binding to ice. *Biochemistry* **1997**, *36* (48), 14652−60.

(2) Clark, M. S.; Worland, M. R. How insects survive the cold: molecular mechanisms-a review. *J. Comp. Physiol., B* **2008**, *178* (8), 917−33. Middleton, A. J.; Brown, A. M.; Davies, P. L.; Walker, V. K. Identification of the ice-binding face of a plant antifreeze protein. *FEBS Lett.* **2009**, *583* (4), 815−9.

(3) Yeh, Y.; Feeney, R. E. Antifreeze Proteins: Structures and Mechanisms of Function. *Chem. Rev.* **1996**, *96* (2), 601−618. Ewart, K. V.; Lin, Q.; Hew, C. L. Structure, function and evolution of antifreeze proteins. *Cell. Mol. Life Sci.* **1999**, *55* (2), 271−83.

(4) Davies, P. L.; Hew, C. L. Biochemistry of fish antifreeze proteins. *FASEB J.* **1990**, *4* (8), 2460−8.

(5) Jia, Z.; Davies, P. L. Antifreeze proteins: an unusual receptor-ligand interaction. *Trends Biochem. Sci.* **2002**, *27* (2), 101−6.

(6) Scotter, A. J.; Marshall, C. B.; Graham, L. A.; Gilbert, J. A.; Garnham, C. P.; Davies, P. L. The basis for hyperactivity of antifreeze proteins. *Cryobiology* **2006**, *53* (2), 229−39.

(7) Ba, Y.; Wongskhaluang, J.; Li, J. Reversible binding of the HPLC6 isoform of type I antifreeze proteins to ice surfaces and the antifreeze mechanism studied by multiple quantum filtering-spin exchange NMR experiment. *J. Am. Chem. Soc.* **2003**, *125* (2), 330−1.

(8) Knight, C. A.; Cheng, C. C.; DeVries, A. L. Adsorption of alpha-helical antifreeze peptides on specific ice crystal surface planes. *Biophys. J.* **1991**, *59* (2), 409−18.

(9) Zhang, W.; Laursen, R. A. Structure-function relationships in a type I antifreeze polypeptide. The role of threonine methyl and hydroxyl groups in antifreeze activity. *J. Biol. Chem.* **1998**, *273* (52), 34806−12.

(10) Wen, D.; Laursen, R. A. A model for binding of an antifreeze polypeptide to ice. *Biophys. J.* **1992**, *63* (6), 1659−62.

(11) Wen, D.; Laursen, R. A. Structure-function relationships in an antifreeze polypeptide. The role of neutral, polar amino acids. *J. Biol. Chem.* **1992**, *267* (20), 14102−8. Yang, D. S.; Sax, M.; Chakrabartty, A.; Hew, C. L. Crystal structure of an antifreeze polypeptide and its mechanistic implications. *Nature* **1988**, *333* (6170), 232−7.

(12) Davies, P. L.; Baardsnes, J.; Kuiper, M. J.; Walker, V. K. Structure and function of antifreeze proteins. *Philos. Trans. R. Soc., B* **2002**, *357* (1423), 927−35.

(13) Wierzbicki, A.; Madura, J. D.; Salmon, C.; Sönnichsen, F. Modeling studies of binding of sea raven type II antifreeze protein to ice. *J. Chem. Inf. Model.* **1997**, *37* (6), 1006−10. Houston, M. E.; Chao, H.; Hodges, R. S.; Sykes, B. D.; Kay, C. M.; Sönnichsen, F. D.; Loewen, M. C.; Davies, P. L. Binding of an oligopeptide to a specific plane of ice. *J. Biol. Chem.* **1998**, *273* (19), 11714−8.

(14) Davies, P. L.; Sykes, B. D. Antifreeze proteins. *Curr. Opin. Struct. Biol.* **1997**, *7* (6), 828−34.

(15) Graham, L. A.; Hobbs, R. S.; Fletcher, G. L.; Davies, P. L. Helical antifreeze proteins have independently evolved in fishes on four occasions. *PLoS One* **2013**, *8* (12), e81285. Graether, S. P.; Slupsky, C. M.; Davies, P. L.; Sykes, B. D. Structure of type I antifreeze protein and mutants in supercooled water. *Biophys. J.* **2001**, *81* (3), 1677−83.

(16) Shah, S. H.; Kar, R. K.; Asmawi, A. A.; Rahman, M. B.; Murad, A. M.; Mahadi, N. M.; Basri, M.; Rahman, R. N.; Salleh, A. B.; Chatterjee, S.; Tejo, B. A.; Bhunia, A. Solution structures, dynamics, and ice growth inhibitory activity of peptide fragments derived from an antarctic yeast protein. *PLoS One* **2012**, *7* (11), e49788.

(17) Sicheri, F.; Yang, D. S. Ice-binding structure and mechanism of an antifreeze protein from winter flounder. *Nature* **1995**, *375* (6530), 427−31.

(18) Liepinsh, E.; Otting, G.; Harding, M. M.; Ward, L. G.; Mackay, J. P.; Haymet, A. D. Solution structure of a hydrophobic analogue of the winter flounder antifreeze protein. *Eur. J. Biochem.* **2002**, *269* (4), 1259−66.

(19) Kwan, A. H.; Fairley, K.; Anderberg, P. I.; Liew, C. W.; Harding, M. M.; Mackay, J. P. Solution structure of a recombinant type I sculpin antifreeze protein. *Biochemistry* **2005**, *44* (6), 1980−8.

(20) Vrbka, L.; Jungwirth, P. Homogeneous freezing of water starts in the subsurface. *J. Phys. Chem. B* **2006**, *110* (37), 18126−9.

(21) Gladich, I.; Roeselová, M. Comparison of selected polarizable and nonpolarizable water models in molecular dynamics simulations of ice I(h). *Phys. Chem. Chem. Phys.* **2012**, *14* (32), 11371−85.

(22) Pereyra, R. G.; Bermúdez di Lorenzo, A. J.; Malaspina, D. C.; Carignano, M. A. On the relation between hydrogen bonds, tetrahedral order and molecular mobility in model water. *Chem. Phys. Lett.* **2012**, *538* (11), 35−38.

(23) Vega, C.; Abascal, J. L. Simulating water with rigid non-polarizable models: a general perspective. *Phys. Chem. Chem. Phys.* **2011**, *13* (44), 19663−88.

(24) Carignano, M. A.; Shepson, P. B.; Szleifer, I. Molecular dynamics simulations of ice growth from supercooled water. *Mol. Phys.* **2005**, *103* (21−23), 2957−2967.

(25) Lu, J.; Qiu, Y.; Baron, R.; Molinero, V. Coarse-Graining of TIP4P/2005, TIP4P-Ew, SPC/E, and TIP3P to monatomic anisotropic water models using relative entropy minimization. *J. Chem. Theory Comput.* **2014**, *10* (9), 4104−4120.

(26) Lindorff-Larsen, K.; Piana, S.; Palmo, K.; Maragakis, P.; Klepeis, J. L.; Dror, R. O.; Shaw, D. E. Improved side-chain torsion potentials for the Amber ff99SB protein force field. *Proteins: Struct., Funct., Genet.* **2010**, *78* (8), 1950−8.

(27) Götz, A. W.; Williamson, M. J.; Xu, D.; Poole, D.; Le Grand, S.; Walker, R. C. Routine Microsecond Molecular Dynamics Simulations with AMBER on GPUs. 1. Generalized Born. *J. Chem. Theory Comput.* **2012**, *8* (5), 1542−1555.

(28) Jorgensen, W. L.; Chandrasekhar, J.; Madura, J. D.; Impey, R. W.; Klein, M. L. Comparison of simple potential functions for simulating liquid water. *J. Chem. Phys.* **1983**, *79* (2), 926−935.

(29) Cerutti, D. S.; Duke, R. E.; Darden, T. A.; Lybrand, T. P. Staggered Mesh Ewald: An extension of the Smooth Particle-Mesh Ewald method adding great versatility. *J. Chem. Theory Comput.* **2009**, *5* (9), 2322.

(30) Plimpton, S. Fast parallel algorithms for short-range molecular dynamics. *J. Comput. Phys.* **1995**, *117* (1), 1−19.

(31) Wang, G. Structures of human host defense cathelicidin LL-37 and its smallest antimicrobial peptide KR-12 in lipid micelles. *J. Biol. Chem.* **2008**, *283* (47), 32637−43.

(32) Dalal, P.; Sönnichsen, F. D. Source of the ice-binding specificity of antifreeze protein type I. *J. Chem. Inf. Model.* **2000**, *40* (5), 1276−84.

(33) Ghoorah, A. W.; Devignes, M. D.; Smaïl-Tabbone, M.; Ritchie, D. W. Protein docking using case-based reasoning. *Proteins: Struct., Funct., Genet.* **2013**, *81* (12), 2150−8.

(34) Abascal, J. L.; Sanz, E.; García Fernández, R.; Vega, C. A potential model for the study of ices and amorphous water: TIP4P/Ice. *J. Chem. Phys.* **2005**, *122* (23), 234511.

(35) Hornak, V.; Abel, R.; Okur, A.; Strockbine, B.; Roitberg, A.; Simmerling, C. Comparison of multiple Amber force fields and development of improved protein backbone parameters. *Proteins: Struct., Funct., Genet.* **2006**, *65* (3), 712−25.

(36) Calvaresi, M.; Höfinger, S.; Zerbetto, F. Local ice melting by an antifreeze protein. *Biomacromolecules* **2012**, *13* (7), 2046−52.

(37) Skjaerven, L.; Martinez, A.; Reuter, N. Principal component and normal mode analysis of proteins; a quantitative comparison using the GroEL subunit. *Proteins: Struct., Funct., Genet.* **2011**, *79* (1), 232−43. Hub, J. S.; de Groot, B. L. Detection of functional modes in protein dynamics. *PLoS Comput. Biol.* **2009**, *5* (8), e1000480.

(38) David, C. C.; Jacobs, D. J. Principal component analysis: a method for determining the essential dynamics of proteins. *Methods Mol. Biol.* **2014**, *1084*, 193−226.

DOI: 10.1021/acs.jpcb.5b04919
J. Phys. Chem. B XXXX, XXX, XXX−XXX

(39) Maisuradze, G. G.; Liwo, A.; Scheraga, H. A. Principal component analysis for protein folding dynamics. *J. Mol. Biol.* **2009**, *385* (1), 312−29.
(40) Pronk, S.; Páll, S.; Schulz, R.; Larsson, P.; Bjelkmar, P.; Apostolov, R.; Shirts, M. R.; Smith, J. C.; Kasson, P. M.; van der Spoel, D.; Hess, B.; Lindahl, E. GROMACS 4.5: a high-throughput and highly parallel open source molecular simulation toolkit. *Bioinformatics* **2013**, *29* (7), 845−54.
(41) Haider, S.; Parkinson, G. N.; Neidle, S. Molecular dynamics and principal components analysis of human telomeric quadruplex multimers. *Biophys. J.* **2008**, *95* (1), 296−311.
(42) Maragliano, L.; Cottone, G.; Cordone, L.; Ciccotti, G. Atomic mean-square displacements in proteins by molecular dynamics: a case for analysis of variance. *Biophys. J.* **2004**, *86* (5), 2765−72.
(43) Hayward, J. A.; Finney, J. L.; Daniel, R. M.; Smith, J. C. Molecular dynamics decomposition of temperature-dependent elastic neutron scattering by a protein solution. *Biophys. J.* **2003**, *85* (2), 679−85.
(44) Atilgan, A. R.; Durell, S. R.; Jernigan, R. L.; Demirel, M. C.; Keskin, O.; Bahar, I. Anisotropy of fluctuation dynamics of proteins with an elastic network model. *Biophys. J.* **2001**, *80* (1), 505−15.
(45) Mu, Y.; Nguyen, P. H.; Stock, G. Energy landscape of a small peptide revealed by dihedral angle principal component analysis. *Proteins: Struct., Funct., Genet.* **2005**, *58* (1), 45−52.
(46) Papaleo, E.; Mereghetti, P.; Fantucci, P.; Grandori, R.; De Gioia, L. Free-energy landscape, principal component analysis, and structural clustering to identify representative conformations from molecular dynamics simulations: the myoglobin case. *J. Mol. Graphics Modell.* **2009**, *27* (8), 889−99.
(47) Durrant, J. D.; McCammon, J. A. HBonanza: a computer algorithm for molecular-dynamics-trajectory hydrogen-bond analysis. *J. Mol. Graphics Modell.* **2011**, *31*, 5−9.
(48) Humphrey, W.; Dalke, A.; Schulten, K. VMD: visual molecular dynamics. *J. Mol. Graphics* **1996**, *14* (1), 33−8 , 27−8..
(49) Seeber, M.; Felline, A.; Raimondi, F.; Muff, S.; Friedman, R.; Rao, F.; Caflisch, A.; Fanelli, F. Wordom: a user-friendly program for the analysis of molecular structures, trajectories, and free energy surfaces. *J. Comput. Chem.* **2011**, *32* (6), 1183−94.
(50) Maisuradze, G. G.; Liwo, A.; Senet, P.; Scheraga, H. A. Local vs global motions in protein folding. *J. Chem. Theory Comput.* **2013**, *9* (7), 2907−2921.
(51) Schirò, G.; Fichou, Y.; Gallat, F. X.; Wood, K.; Gabel, F.; Moulin, M.; Härtlein, M.; Heyden, M.; Colletier, J. P.; Orecchini, A.; Paciaroni, A.; Wuttke, J.; Tobias, D. J.; Weik, M. Translational diffusion of hydration water correlates with functional motions in folded and intrinsically disordered proteins. *Nat. Commun.* **2015**, *6*, 6490.
(52) Todde, G.; Whitman, C.; Hovmöller, S.; Laaksonen, A. Induced ice melting by the snow flea antifreeze protein from molecular dynamics simulations. *J. Phys. Chem. B* **2014**, *118* (47), 13527−34.
(53) Ba, Y.; Mao, Y.; Galdino, L.; Günsen, Z. Effects of a type I antifreeze protein (AFP) on the melting of frozen AFP and AFP +solute aqueous solutions studied by NMR microimaging experiment. *J. Biol. Phys.* **2013**, *39* (1), 131−44.
(54) Todde, G.; Hovmöller, S.; Laaksonen, A. Influence of antifreeze proteins on the ice/water interface. *J. Phys. Chem. B* **2015**, *119* (8), 3407−13.
(55) McCammon, J. A.; Harvey, S. C. *Dynamics of Proteins and Nucleic Acids*; Cambridge University Press: Cambridge, U.K., 1988.
(56) Shen, J.; Zhang, W.; Fang, H.; Perkins, R.; Tong, W.; Hong, H. Homology modeling, molecular docking, and molecular dynamics simulations elucidated α-fetoprotein binding modes. *BMC Bioinf.* **2013**, *14* (Suppl.14), S6.
(57) Kundu, S.; Roy, D. Temperature-induced unfolding pathway of a type III antifreeze protein: insight from molecular dynamics simulation. *J. Mol. Graphics Modell.* **2008**, *27* (1), 88−94.

DOI: 10.1021/acs.jpcb.5b04919
J. Phys. Chem. B XXXX, XXX, XXX−XXX